Adaptive Multiresolution Simulation of Waves in Electrocardiology

Raimund Bürger and Ricardo Ruiz-Baier

Abstract A new fully adaptive multiresolution method is applied for the simulation of the complex dynamics of waves in excitable media in electrocardiology, where the membrane kinetics are given by the Aliev–Panfilov or Luo–Rudy II models. Numerical experiments show that the automatical adaptation strategy tracks the spatio-temporal pattern accurately at a substantially reduced computational cost if compared with fine-grid simulations. The nonlinear dynamics of complex multiscale patterns can thus be computed efficiently, also in the chaotic and turbulent regime which are currently beyond the frontiers of methods using regular discretizations.

1 Introduction

Nonlinear reaction-diffusion systems are widely used models of excitable chemical and biological media that usually exhibit rich spatio-temporal multiscale dynamics. Even in homogeneous media, nontrivial spatial structures (pulses, fronts, spiral waves and others) can emerge, and an impulse over a certain threshold initiates a wave of activity moving across the excitable medium. One of the most studied applications of such waves is the propagation of electrical activity in cardiac tissue. This phenomenon involves the interaction of different ion species across a combination of active and passive ion channels and diffusion of charge through a heterogeneous substrate with dynamically changing conductances.

It is the purpose of this contribution to provide further support for the adaptive multiresolution method for excitable media described in [4] by two new, original

R. Bürger (✉)
CI^{2}MA and Departamento de Ingeniería Matemática, Universidad de Concepción, Casilla 160-C, Concepción, Chile
e-mail: rburger@ing-mat.udec.cl

R. Ruiz-Baier
Modeling and Scientific Computing IACS-CMCS, École Polytechnique Fédérale de Lausanne EPFL, Station 8, CH-1015 Lausanne, Switzerland
e-mail: ricardo.ruiz@epfl.ch

G. Kreiss et al. (eds.), *Numerical Mathematics and Advanced Applications 2009*,
DOI 10.1007/978-3-642-11795-4_20,

numerical examples for the Aliev–Panfilov (AP) and Luo–Rudy II (LRII) models in electrocardiology. The new feature of the example for the AP model is an implanted obstacle, while the LRII model is remarkably more involved than the models used in [4] since it includes a vector of seven gating variables, not just a scalar one.

We first consider a spatially two-dimensional model of waves in excitable media given by a reaction-diffusion system of the generic form

$$\partial_t u = \Delta A(u) + f(u,v), \quad \partial_t v = g(u,v), \quad (x,t) \in Q_T := \Omega \times [0,T], \tag{1}$$

where $\Omega \subset \mathbb{R}^2$ is an open, bounded, connected polygonal domain with boundary $\partial\Omega$, along with zero-flux boundary and initial conditions. The unknowns are the excitation and recovery variables u and v, which vary on fast and slow time scales, respectively. The functions f and g express the local reaction kinetics and A is a diffusion coefficient to be defined later.

The model by Aliev and Panfilov for propagation in cardiac tissue [1] is employed as the first of two specific examples. It consists in (1) along with

$$\begin{aligned} f(u,v) &= \{-C_1 u \text{ if } u < \rho_1,\ C_2 u + a \text{ if } u \in [\rho_1,\rho_2],\ C_3(1-u) \text{ if } u > \rho_2\} - v, \\ g(u,v) &= (ku - v) \cdot \{\eta_1 \text{ if } u < \rho_2,\ \eta_2 \text{ if } u > \rho_2,\ \eta_3 \text{ if } u < \rho_1 \text{ and } v < v_1\}, \end{aligned} \tag{2}$$

where $C_1, C_2, C_3, \eta_1, \eta_2, \eta_3, v_1$ and k are certain dimensionless parameters. The AP model (2) models the electrical activity in ventricular tissue more accurately than the well-known FitzHugh–Nagumo model (see [7]).

The second example is the LRII model [8] coupled with a monodomain description of the electrical wave propagation. It has the general form

$$\partial_t u = D\Delta u + f(u,\mathbf{v}) + I_{\text{ext}}(x,t), \quad \partial_t \mathbf{v} = g(u,\mathbf{v}), \quad (x,t) \in Q_T := \Omega \times [0,T], \tag{3}$$

where u is the membrane potential, $\mathbf{v} = (K_1, X, h, j, m, f, d)^{\mathrm{T}}$ is the vector of dimensionless ion-channel gating variables, and the total ionic current density

$$f(u,\mathbf{v}) = I_{\text{Na}}(u,\mathbf{v}) + I_{\text{si}}(u,\mathbf{v}) + I_{\text{K}}(u,\mathbf{v}) + I_{\text{K}_1}(u,\mathbf{v}) + I_{\text{K}_\text{p}}(u) + I_{\text{b}}(u)$$

is the sum of a fast inward sodium current I_{Na}, a slow inward current I_{si}, a time-dependent potassium slow outward current I_{K}, an outward potassium current I_{K_1}, a plateau potassium current I_{K_p}, and a total background current I_{b}:

$$\begin{aligned} I_{\text{Na}} &= G_{\text{Na}} m^3 h j (u - E_{\text{Na}}), & I_{\text{si}} &= G_{\text{si}} d f (u - E_{\text{si}}), & I_{\text{K}} &= G_{\text{K}} X X_i (u - E_{\text{K}}), \\ I_{\text{K}_1} &= G_{\text{K}_1} K_{1\infty} (u - E_{\text{K}_1}), & I_{\text{K}_\text{p}} &= G_{\text{K}_\text{p}} K_{\text{p}} (u - E_{\text{K}_\text{p}}), & I_{\text{b}} &= 0.03921(u + 59.87) \end{aligned}$$

with $G_{\text{Na}} = 23, G_{\text{si}} = 0.07, G_{\text{K}} = 0.705, G_{\text{K}_1} = 0.604, G_{\text{K}_\text{p}} = 0.0183 (\text{in mS cm}^{-2})$, $E_{\text{Na}} = 54.4$, $E_{\text{K}} = -77$, $E_{\text{K}_1} = -87.26$, $E_{\text{K}_\text{p}} = -87.26$, $E_b = -59.87$ (in mV). In addition, $E_{\text{si}} = 7.7 - 13.0287 \ln[\text{Ca}]_+$. The calcium ionic concentration satisfies

the Nernst equilibrium $d_t[\mathrm{Ca}]_+ = -10^{-4} I_{\mathrm{si}} + G_{\mathrm{si}}(10^{-4} - [\mathrm{Ca}]_+)$, and all gate variables $\rho = h, j, m, d, f, X, K_1$ evolve according to $d_t \rho = \alpha_\rho(u)(1-\rho) - \beta_\rho(u)\rho$, which precisely corresponds to the second equation in (3). Here, $\alpha_\rho(u)$ and $\beta_\rho(u)$ define the opening and closure rate of the gates, which are given by $\alpha_h = \alpha_j = 0$ for $u \geq -40\,\mathrm{mV}$, $\alpha_h = 0.135\mathrm{e}^{-0.147(u+80)}$ for $u < -40\,\mathrm{mV}$, and

$$\beta_h = \begin{cases} 3.56\mathrm{e}^{0.079u} + 3.1 \times 10^5 \mathrm{e}^{0.35u} & \text{for } u < -40\,\mathrm{mV}, \\ (0.13 + 0.13\mathrm{e}^{-0.09(u+10.66)})^{-1} & \text{otherwise}, \end{cases}$$

$$\alpha_j = (u + 37.8)\frac{\mathrm{e}^{0.2} + 2.7 \times 10^{-10}\mathrm{e}^{-0.04u}}{-7.87 \times 10^{-6}(1 + \mathrm{e}^{0.3(u+79.2)})} \quad \text{for } u < -40\,\mathrm{mV},$$

$$\beta_j = \begin{cases} 0.1212\mathrm{e}^{-0.01052u}(1 + \mathrm{e}^{-0.1378(u+40.14)})^{-1} & \text{for } u < -40\,\mathrm{mV}, \\ 0.3\mathrm{e}^{-2.535\times 10^{-7}u}(1 + \mathrm{e}^{-0.1(u+32)})^{-1} & \text{otherwise}, \end{cases}$$

$$\alpha_{K_1} = \frac{1.2}{1 + \mathrm{e}^{0.2385(u - E_{K_1} - 59.215)}}, \alpha_m = \frac{0.32(u + 47.13)}{1 - \mathrm{e}^{-0.1(u+47.13)}}, \beta_m = 0.08\mathrm{e}^{-0.0909u},$$

$$\alpha_d = \frac{0.095\mathrm{e}^{-0.01(u-5)}}{1 + \mathrm{e}^{-0.072(u-5)}}, \quad \beta_d = \frac{0.07\mathrm{e}^{-0.02(u+44)}}{1 + \mathrm{e}^{0.05(u+44)}}, \quad \alpha_f = \frac{0.012\mathrm{e}^{-0.008(u+28)}}{1 + \mathrm{e}^{0.15(u+28)}},$$

$$\beta_f = \frac{0.0065\mathrm{e}^{-0.02(u+30)}}{1 + \mathrm{e}^{-0.2(u+30)}}, \alpha_X = \frac{0.0005\mathrm{e}^{0.083(u+50)}}{1 + \mathrm{e}^{0.057(u+50)}}, \beta_X = \frac{0.0013\mathrm{e}^{-0.06(u+20)}}{1 + \mathrm{e}^{-0.04(u+20)}},$$

$$\beta_{K_1} = \frac{0.4912\mathrm{e}^{0.08(u - E_{K_1} + 5.476)}}{1 + \mathrm{e}^{-0.5143(u - E_{K_1} + 4.75)}} + \mathrm{e}^{0.0618(u - E_{K_1} - 594.31)}.$$

The gating variables X_i, K_p are assumed to rapidly reach a steady state, and therefore to depend only on the potential u. We set $X_i(u) = 1$ for $u \leq -100\,\mathrm{mV}$ and

$$X_i = (2.837\mathrm{e}^{0.04(u+77)} - 1)((u + 77)\mathrm{e}^{0.04(u+35)})^{-1} \quad \text{for } u > -100\,\mathrm{mV},$$
$$K_p = \left(1 + \mathrm{e}^{0.1672(7.488-u)}\right)^{-1}.$$

For overviews on multiresolution techniques for related problems, see [5, 9, 10]; references to other techniques to solve the system (1) are given in [4].

The remainder of the paper is organized as follows. In Sect. 2 we recall the numerical method for solving (1) on uniform fine meshes. This method is a classical finite volume (FV) scheme with a first-order Euler time discretization, and plays the role of a *reference numerical scheme*, i.e., it approximates the solution of (1) on a uniform mesh. In Sect. 3 we outline the MR procedure, which allows to construct space adaptive schemes based on the reference method (for details, see [4, 10]). The numerical results are presented in Sect. 4.

2 Reference Numerical Scheme

We consider a standard admissible mesh for $\Omega \subset \mathbb{R}^2$ formed by a family $\mathscr{T}$ of control volumes K of maximum diameter h and a family of points $(x_K)_{K\in\mathscr{T}}$, where x_K is the center of K. We let $N(K)$ denote the set of neighbors of K which share a common edge with K. Here $\mathscr{E}_{\text{int}}(K)$ is the set of edges of K in the interior of Ω and $\mathscr{E}_{\text{ext}}(K)$ the set of edges of K lying on the boundary $\partial\Omega$. For all $L \in N(K)$, $d(K,L)$ denotes the distance between x_K and x_L, and we denote by $\sigma = K|L$ ($\sigma = K|\partial\Omega$, respectively) the interface between K and L (between K and $\partial\Omega$, respectively). Moreover, $|K|$ stands for the two-dimensional measure of K and $|\sigma|$ for the one-dimensional measure of σ. Numerical fluxes on all edges σ are defined as by $F_{K,\sigma} = \tau_\sigma(u_L - u_K)$ for $\sigma = K|L \in \mathscr{E}_{\text{int}}(K)$ and $F_{K,\sigma} = 0$ for $\sigma \in \mathscr{E}_{\text{ext}}(K)$, which includes the zero-flux boundary conditions and where the transmissibility coefficients τ_σ are defined by $\tau_\sigma := |\sigma|/|d(K,L)|$ for $\sigma = K|L \in \mathscr{E}_{\text{int}}(K)$. We set $t^n := n\Delta t$ for $n = 0,\dots,N = \lceil T/\Delta t\rceil$. We define $f_K^n := f(u_K^n, v_K^n)$, $g_K^n := g(u_K^n, v_K^n)$, $u_K^0 := |K|^{-1}\int_K u_0(x)\mathrm{d}x$ and $v_K^0 := |K|^{-1}\int_K v_0(x)\mathrm{d}x$. To advance the numerical solution from t^n to $t^{n+1} = t^n + \Delta t$, we use the following finite volume scheme: Given u_K^n, v_K^n for all $K \in \mathscr{T}$, determine u_K^{n+1} and v_K^{n+1} from

$$|K|\Delta t^{-1}\big(u_K^{n+1} - u_K^n\big) + \textstyle\sum_{\sigma\in\mathscr{E}_{\text{int}}(K)\cup\mathscr{E}_{\text{ext}}(K)}\tau_\sigma\left(A\big(u_L^{n+1}\big) - A\big(u_K^{n+1}\big)\right) = |K| f_K^n, \tag{4}$$

$$\Delta t^{-1}\big(v_K^{n+1} - v_K^n\big) = g_K^n \ \text{ for all } K \in \mathscr{T}. \tag{5}$$

A CFL stability condition for the scheme (4) and (5) is given by

$$\Delta t h^{-1} \max_{K\in\mathscr{T},\, t^n<T}\left(\big|f_{u,K}^n\big| + \big|f_{v,K}^n\big| + \big|g_{u,K}^n\big| + \big|g_{v,K}^n\big|\right) + 4D\Delta t h^{-3} \le 1. \tag{6}$$

The resulting FV scheme produces a unique numerical solution. Solutions converge to a weak solution of (1) as the discretization parameters tend to zero [6].

3 Adaptivity: Multiresolution Framework

To be concise, we only consider Cartesian meshes on $\overline{\Omega} = [0,1]^2$, but the MR analysis could be carried out for more general meshes (see, e.g., [9]). We start by determining a nested mesh hierarchy $\mathscr{T}_0 \subset \cdots \subset \mathscr{T}_H$, using a partition of Ω. Each grid $\mathscr{T}_l$ is formed by the control volumes K^l on each level $l = 0,\dots,H$, where $l = 0$ corresponds to the coarsest and $l = H$ to the finest level. The *refinement sets* are defined by $\mathscr{M}_{K^l} := \{L_i^{l+1}\}_i$, where $\overline{K^l} := L_1^{l+1} \cup \cdots \cup L_{m_l}^{l+1}$, $m_l := \#\mathscr{M}_{K^l}$, where L_i^{l+1} is a control volume at level $l+1$, $L_i^{l+1} \subset K^l$. For $x \in K^l$ the *scale box function* is defined as $\tilde{\varphi}_{K^l}(x) := |K^l|^{-1}\chi_{K^l}(x)$, and therefore

the average of any function $u(\cdot,t) \in L^1(\Omega)$ on K^l can be expressed as the inner product $u_{K^l} := \langle u, \tilde{\varphi}_{K^l} \rangle_{L^1(\Omega)}$.

Cell averages and box functions satisfy the two-level relation

$$u_{K^l} = \sum_{L_i^{l+1} \in \mathscr{M}_{K^l}} |L_i^{l+1}||K^l|^{-1} u_{L_i^{l+1}}, \quad \tilde{\varphi}_{K^l} = \sum_{L_i^{l+1} \in \mathscr{M}_{K^l}} |L_i^{l+1}||K^l|^{-1} \tilde{\varphi}_{L_i^{l+1}}, \tag{7}$$

which defines a projection operator needed to move from finer to coarser levels. There is a transformation between the cell averages on level $l = H$ and the cell averages on level $l = 0$ plus a series of detail coefficients. This relation defines a prediction operator needed to move from coarser to finer resolution levels. A polynomial prediction is chosen, which in the particular case of Cartesian meshes is defined by $\tilde{u}_{L_i,l+1} = u_{L,l} - Q_x - Q_y + Q_{xy}$ for $i = 1, \ldots, \#\mathscr{M}_{K^l}$, where Q_x, Q_y and Q_{xy} are standard polynomial interpolators applied to the neighbors and diagonal neighbors of the control volume L^l, see [2–4, 10].

The error induced by the prediction operator at the cell K^l is defined as the difference between the cell average and the predicted value, i.e., $d_{K^l} := u_{K^l} - \tilde{u}_{K^l}$, and we may also write $d_{K^l,j} := \langle u, \tilde{\psi}_{K^l,j} \rangle$ for $j = 1, \ldots, \#\mathscr{M}_{K^l}$. For a multicomponent solution (u, v), on each cell K^l we compute for the refinement stages

$$d_{K^l} = \min\{|u_{K^l} - \tilde{u}_{K^l}|, |v_{K^l} - \tilde{v}_{K^l}|\}, \tag{8}$$

and use the maximum for the coarsening stages of the algorithm.

Roughly speaking, the more regular a function u is over K^l, the smaller is the corresponding detail coefficient. This motivates the so-called *thresholding* procedure, which consists in discarding all control volumes corresponding to details that are smaller in absolute value than a level-dependent tolerance ε_l. Choosing ε_l too small or too large will make the MR device inefficient (the compression rate is poor) or deteriorate the quality of the solution due to large thresholding errors, respectively.

For problems considered in [5] and [10], the reference scheme has a known order of convergence in space ($\alpha = 1/2$ and $\alpha = 2$ respectively). The latter constant is at present unknown for FV discretizations of degenerate parabolic equations. However, in [2, 3] we found that a methodology based on the ideas of [5, 10] can also be successfully applied to degenerate reaction-diffusion systems when α is a convergence rate obtained from numerical experiments. This approach is also applied here. Let us denote by α the experimental convergence rate of (4) and (5), which by means of standard preliminary computations (see e.g., [2]) we have found to be $\alpha = 1.2$.

Let the level-dependent tolerances ε_l be given by $\varepsilon_l = 2^{2(l-H)}\varepsilon_R$ for $l = 0, \ldots, H$. If the general time evolution operator is L^1-contractive and the reference numerical scheme is stable in the sense of (6) and the reference tolerance ε_R is set to

$$\varepsilon_{\mathrm{R}} = C\,\frac{2^{-(\alpha+2)H}}{|\Omega|\max\limits_{K\in\mathscr{T},\, t^n<T}\left(\left|f^n_{u,K}\right|+\left|f^n_{v,K}\right|+\left|g^n_{u,K}\right|+\left|g^n_{v,K}\right|\right)+D|\Omega|^{3/2}2^{2+H}}, \tag{9}$$

then the error due to thresholding is of the same order as the discretization error, and therefore the order of the underlying scheme is preserved. The constant C in (9) has to be determined by test calculations on a uniform grid (and possibly in one space dimension only), prior to the proper MR simulation, see e.g., [4, Example 4].

We organize the cell averages and corresponding details at different levels in a *dynamic graded tree*. The root is the basis of the tree. A parent node has four sons, and the sons of the same parent are called brothers. A node without sons is a leaf. A given node has $s' = 2$ nearest neighbors in each spatial direction, needed for the computation of the fluxes of leaves; if these neighbors do not exist, we create them as virtual leaves. Brothers are also considered nearest neighbors. We denote by Λ the set of all nodes of the tree and by $\mathscr{L}(\Lambda)$ the restriction of Λ to the leaves. We apply this MR representation to the spatial part of the function $\mathbf{u} = (u, v)$, which corresponds to the numerical solution of the underlying problem for each time step, so we need to update the tree structure for the proper representation of the solution during the evolution. To this end, we apply the above thresholding strategy, but always ensure the graded tree structure of the data.

We define the *data compression rate* $\eta := N/(2^{-(2H)}N + \#\mathscr{L}(\Lambda))$, where N is the number of control volumes in the full finest grid at level $l = H$, and $\#\mathscr{L}(\Lambda)$ is the number of leaves. The *speed-up* between the CPU times of the numerical solutions obtained by the FV and MR methods is defined by $\mathscr{V} := \mathrm{CPU\,time_{FV}}/\mathrm{CPUtime_{MR}}$.

4 Numerical Results

Example 1 corresponds to the AP model (1), (2) on $\Omega = (0, 256)^2$ (in millimeters). The physiological parameters are $\rho_1 = 0.0026$, $\rho_2 = 0.837$, $C_1 = 20$, $C_2 = 3$, $C_3 = 15$, $a = 0.06$, $k = 3$, $\nu_1 = 1.8$, $\eta_1 = 0.01$, $\eta_2 = 1.0$, $\eta_3 = 0.3$, $D = 2\,\mathrm{cm}^2/\mathrm{s}$ [1, 11]. We consider an inhomogeneity in the conductivity of the medium by setting $A(u) = 0$ if $\|(x - 230, y - 160)\| \le 20$ and $A(u) = Du$ otherwise. This circular obstacle could represent a scar on the cardiac tissue. For simplicity, we impose no-flux boundary conditions on the border of the obstacle. We let $u_0 = 0.9$ if $x \le 128$ and $y = 129$, $u_0 = 0$ otherwise, $v_0 = 2$ if $y \le 128$ and $v_0 = 0$ otherwise.

Figure 1 shows the evolution of u for this example. Clearly, the spiral turbulence, which otherwise dominates the evolution of the system, remains away from the obstacle, and the MR-based adaptive mesh adequately captures the excitation fronts. From (9) we obtain $\varepsilon_{\mathrm{R}} = 4.50 \times 10^{-4}$, and this value indeed produces experimental rates of convergence of about $h^{1.2}$ (see the upper part of Table 1).

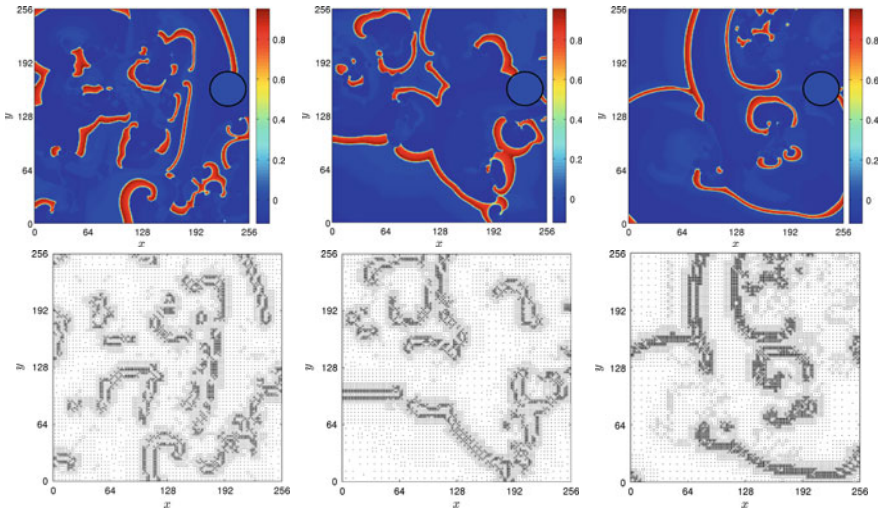

Fig. 1 Example 1. Aliev–Panfilov model: transmembrane potential u and corresponding graded tree structure for times (from *left* to *right*) $t = 0.1$ s, $t = 1$ s and $t = 1.4$ s

Table 1 Examples 1 and 2. Convergence history in different norms, and compression rates

Ex.	h_H	L^1-error	L^1-rate	L^2-error	L^2-rate	$L^\infty-$error	$L^\infty-$rate	η	$\mathscr{V}$
	2^2	4.31×10^{-2}	–	3.44×10^{-2}	–	8.11×10^{-2}	–	9.4112	9.4293
	2^1	1.83×10^{-2}	1.2371	1.47×10^{-2}	1.2309	3.43×10^{-2}	1.2407	11.0309	13.9917
1	2^0	7.92×10^{-3}	1.2133	6.12×10^{-3}	1.2632	1.45×10^{-2}	1.2386	13.1710	17.4209
	2^{-1}	3.31×10^{-3}	1.2482	2.64×10^{-3}	1.2238	6.11×10^{-3}	1.2490	17.2136	20.8701
	2^{-2}	1.42×10^{-3}	1.2710	1.13×10^{-3}	1.2461	2.60×10^{-3}	1.2589	21.8554	28.0526
	2^{-5}	6.72×10^{-2}	–	5.29×10^{-2}	–	8.15×10^{-2}	–	7.3650	11.7923
	2^{-6}	2.99×10^{-2}	1.1675	2.35×10^{-2}	1.1704	3.62×10^{-2}	1.1715	9.8097	16.6464
2	2^{-7}	1.31×10^{-2}	1.1967	1.03×10^{-2}	1.1928	1.59×10^{-2}	1.1899	12.3146	21.9165
	2^{-8}	5.72×10^{-3}	1.2033	4.51×10^{-3}	1.2049	6.91×10^{-3}	1.2031	15.1622	28.1796
	2^{-9}	2.53×10^{-3}	1.2089	1.90×10^{-3}	1.2160	3.03×10^{-3}	1.2097	20.7391	34.1880

In Example 2 we employ the LRII model (3) on $\Omega = (0, 8)^2$ (in centimeters) with $D = 1.25 \times 10^{-3}\,\mathrm{cm}^2/\mathrm{ms}$. Initially the tissue has an constant rest state $u = -84\,\mathrm{mV}$. To produce computational fibrillation, a reentrant wave is generated using a wavefront which after 0.25 ms is broken at the center of the domain. The external stimuli $I_{\mathrm{ext}} = -100\,\mu\mathrm{A}/\mathrm{cm}^2$ for $t < 1\,\mathrm{ms}$ and $x < 0.2\,\mathrm{cm}$, and $I_{\mathrm{ext}} = -50\,\mu\mathrm{A}/\mathrm{cm}^2$ for $315\,\mathrm{ms} < t < 316\,\mathrm{ms}$, $x \geq 4.5\,\mathrm{cm}$, $y \geq 4.5\,\mathrm{cm}$ are applied. The domain is initially discretized in $N = 256^2$ control volumes, the time step is set according to (6), and we use $\varepsilon_{\mathrm{R}} = 5.15 \times 10^{-3}$. The initial value for [Ca] is 2×10^{-4} mmol/L.

Figure 2 shows the numerical solution for u along with the corresponding representation of the leaves of the dynamic graded tree, which form the adaptive mesh generated by the MR algorithm. We observe that the wave created by the first

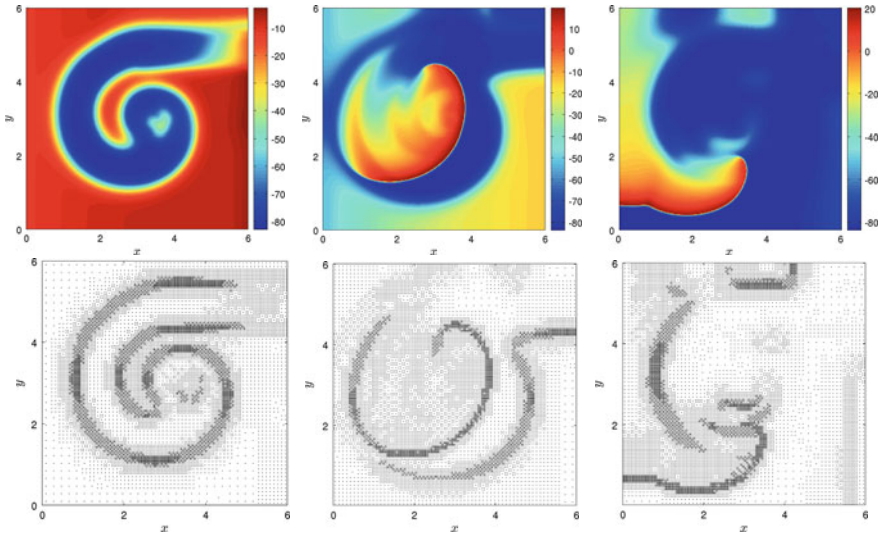

Fig. 2 Example 2. LRII model: transmembrane potential u and corresponding graded tree structure for times (from *left* to *right*) $t = 100$ ms, $t = 200$ ms and $t = 300$ ms

stimulus applied at the left border of the domain propagates to the right, and after applying the second stimulus, a rotating spiral wave forms. The MR device performs an automatic refinement/coarsening stage to accurately capture the high gradient fronts.

The lower half of Table 1 reports the convergence history of the MR method together with η and $\mathscr{V}$ (corresponding to $t = 200$). As in Example 1, the errors maintain a convergence rate of around $h^{1.2}$ and $\mathscr{V}$ grows linearly with the number of control volumes in the finest mesh N_H, and η reaches similar levels as in Example 1. In the reference scheme, for Example 1, most of the computational time is spent in resolving the diffusive part, while for Example 2, the stiffness of the ODE system for the gating variables requires the major part of the overall computational cost. In contrast to Example 1 and other multicomponent problems (see e.g., [2]), we here do not use (8) for the refinement and coarsening procedures, but only use the information on u, i.e., the whole system is evolved over a mesh whose construction is based on the local regularity of u. This simplification avoids the computation of details for all seven gating variables while maintaining a reasonable accuracy level.

Acknowledgements RB is supported by Fondecyt proj. 1090456, Fondap proj. 15000001, and BASAL project CMM, U. de Chile and Centro de Investigación en Ingeniería Matemática (CI^{2}MA), U. de Concepción. RR is supported by the Europ. Res. Council Advanced Grant "Mathcard, Mathematical Modelling and Simulation of the Cardiovascular System", proj. ERC-2008-AdG 227058.

References

1. Aliev, R.R., Panfilov, A.V.: A simple two-variable model of cardiac excitation. Chaos Solit. Fract. **7**, 293–301 (1996)
2. Bendahmane, M., Bürger, R., Ruiz-Baier, R.: A multiresolution space-time adaptive scheme for the bidomain model in electrocardiology. Numer. Meth. Partial Diff. Eqns. (to appear)
3. Bendahmane, M., Bürger, R., Ruiz-Baier, R., Schneider, K.: Adaptive multiresolution schemes with local time stepping for two-dimensional degenerate reaction-diffusion systems. Appl. Numer. Math. **59**, 1668–1692 (2009)
4. Bürger, R., Ruiz-Baier, R., Schneider, K.: Adaptive multiresolution methods for the simulation of waves in excitable media. J. Sci. Comput. **43**, 261–290 (2010)
5. Cohen, A., Kaber, S., Müller, S., Postel, M.: Fully adaptive multiresolution finite volume schemes for conservation laws. Math. Comp. **72**, 183–225 (2003)
6. Eymard, R., Gallouët, T., Herbin, R.: Finite Volume Methods. In Ciarlet, P.G., and Lions, J.L. (eds.), Handbook of Numerical Analysis, vol. VII. North-Holland, Amsterdam, pp. 713–1020 (2000)
7. Keener, J., Sneyd, J.: Mathematical Physiology I: Cellular Physiology II: Systems Physiology, Second Edition. Springer, New York (2009)
8. Luo, C., Rudy Y.: A dynamic model of the cardiac ventricular action potential – simulations of ionic currents and concentration changes. Circ. Res. **74**, 1071–1097 (1994)
9. Müller, S.: Adaptive Multiscale Schemes for Conservation Laws. Springer, Berlin (2003)
10. Roussel, O., Schneider, K., Tsigulin, A., Bockhorn, H.: A conservative fully adaptive multiresolution algorithm for parabolic PDEs. J. Comput. Phys. **188**, 493–523 (2003)
11. Shajahan, T.K., Sinha, S., Pandit, R.: Spiral-wave dynamics depends sensitively on inhomogeneities in mathematical models of ventricular tissue. Phys. Rev. E **75**, 011929 (2007)